NASA Technical Memorandum 106198
AIAA–93–2381

IN-07
169430
P.13

Comparison of Reacting and Non-Reacting Shear Layers at a High Subsonic Mach Number

C.T. Chang and C.J. Marek
Lewis Research Center
Cleveland, Ohio

C. Wey
Sverdrup Technology, Inc.
Lewis Research Center Group
Brook Park, Ohio

R.A. Jones
Rensselaer Polytechnic Institute
Troy, New York

and

M.J. Smith
Purdue University
West Lafayette, Indiana

NASA

COMPARISON OF REACTING AND NON-REACTING SHEAR LAYERS AT A HIGH SUBSONIC MACH NUMBER

C.T. Chang* and C.J. Marek**
National Aeronautics and Space Administration
Lewis Research Center
Cleveland, Ohio 44135

C. Wey[†]
Sverdrup Technology, Inc.
Lewis Research Center Group
Brook Park, Ohio 44142

R.A. Jones[‡]
Dept. of Mechanical Engineering, Aeronautical Engineering, and Mechanics
Rensselaer Polytechnic Institute
Troy, New York 12180

and

M.J. Smith[§]
School of Chemical Engineering
Purdue University
West Lafayette, Indiana 47907

ABSTRACT

The flow field in a hydrogen-fueled planar reacting shear layer was measured with an LDV system and is compared with a similar air to air case without combustion. Measurements were made with a speed ratio of 0.34 with the high-speed stream at Mach 0.71. They show that the shear layer with reaction grows faster than one without, and both cases are within the range of data scatter presented by the established database. The coupling between the streamwise and the cross-stream turbulence components inside the shear layers is low, and reaction only increased it slightly. However, a more organized pattern of the Reynolds Stress is present in the reacting shear layer, possibly as a result of larger scale structure formation in the layer associated with heat release.

NOMENCLATURE

x   Streamwise coordinate, origin at splitter plate tip, [mm]

y   Cross-stream coordinate, origin at splitter plate tip, [mm]

u,v   Instantaneous streamwise and cross-stream speed components, in x and y directions, [m/s]

U,V   Streamwise and cross-stream mean flow [m/s]

u',v'   Streamwise and cross-stream turbulence intensity, RMS, [m/s]

T   Thermocouple temperature, not corrected for radiative loss, [K]

M_c Convective Mach number

1,2   Subscripts denote air side (lower duct) and fuel side (upper duct) flow parameters.

U_m Median streamwise speed, $(U_1+U_2)/2$

U_c Convective speed, speed at which dynamic pressure from the two streams are equal.

y_m Location at each streamwise station where U_m exists.

δ_ω Velocity vorticity thickness at each streamwise station.

1. INTRODUCTION

In a 1985 survey of past research done on turbulent reacting flows, Strahle and Lekoudis[1] noted that much more turbulence and reacting data within a planar reacting shear layer at higher Reynolds number conditions are needed, especially using non-intrusive laser diagnostics. This is especially important since large deviations exists between experimental data and computational models in this area, for example, that of Hermanson[2] and the computations using the standard two equation turbulence-dissipation model[3]. Since Hermanson's data set did not include the magnitude of the fluctuations, it was difficult to determine the cause of the difference, here shown in Figure 1A.

When the computer model was expanded to include generation terms from velocity and concentration coupling by adding eight more differential equations and eleven more constants[4], the comparison was much better, here shown in Figure 1B. However, the question is whether these constants are universal over a large range, especially in the higher speed range applicable to modern thermal power systems.

There are data available on reacting planar shear layers, but most of them are at low velocities. Batt[5] studied a wall jet mixing into still air via dilute nitrogen tetroxide dissociation using seeded flow photography. Even at the low speeds of 15 and 7 m/s, he observed that turbulent motion in a shear layer is characterized more by random 3-D motion than by 2-D coherent structures. He inferred a turbulent Prandtl number of 0.5 from his reacting shear layers.

Wallace[6] studied the shear layer in a duct reacting dilute

---

* Research Scientist, AIAA member
** Senior Research Scientist, AIAA member
† Research Scientist
‡ Graduate Student, RPI.
§ Undergraduate Senior, Purdue U.

nitric oxide with ozone in helium, nitrogen, and argon using simultaneous shadowgraphs. His main conclusion was that the reaction thermicity caused the overall growth rate to be unchanged, with the growth due to thermal expansion being countered by entrainment rate (and hence mixedness) reductions by the attenuation of the smaller scales which was visible from his shadowgraphs. However, as in Batt's case, his flow speed was about 25 m/s, much slower than the common speed in combustors. The relevant question to ask, then, is whether the same phenomena also exists at the higher speed regimes.

With the resurgence in high-speed flow research, the need to understand mixing and reaction in compressible flows is even more pressing, and major efforts are being carried out in supersonic flows to address the issues involved in planar shear layers[7,8,9]. However, a gap exists in the high-subsonic range where no reacting data exists, which especially is applicable to gas turbine combustors and internal rocket flows. This report addresses this regime and introduces a set of benchmark data to be used for computational fluid dynamics in reacting fluid flow.

For this purpose, a new continuous flow, reacting shear layer facility was built at NASA Lewis to provide a complete set of data, including boundary and initial conditions for computational modeling verification and development. It presents a velocity and temperature data set obtained in May and June of 1992 for CFD code validation. Presented here are the mean velocities, turbulence intensities, and the temperature profiles measured for a planar shear layer reacting hot air with hydrogen (diluted with nitrogen). A non-reacting shear layer substituting air for the hydrogen stream was also measured for direct comparison. The high-speed, high temperature air side flowed at Mach 0.71, and the speed ratio is 0.34. The Reynolds number at x=300 mm based on the average viscosity, local layer thickness, and the slip speed, is about 1.8×10^5. The speeds involved are about an order of magnitude larger than the previously available database. Flow field velocities were measured with a two component laser Doppler velocimeter and temperatures were measured with platinum wire thermocouples.

2. EXPERIMENT DESCRIPTION

2.1 FLOW FACILITY

A continuously operating combusting shear layer wind tunnel was built to provide capability for optical diagnostics of the phenomenon[10]. Figure 2 contains the schematic and approximate dimensions of the experiment.

A compressor-supplied non-vitiating heater provides 1.9 kg/s of air at 820 K which throttled down to 1 atmosphere pressure. This air flow is introduced into the test section below the horizontal splitter plate. The fuel stream is heated to 300 K using a steam heat exchanger and is introduced into the test section above the same plate. This stream consists of hydrogen with a flow rate of 0.032 kg/s diluted with nitrogen of 1.2 kg/s. The two streams enter the test section horizontally and parallel to each other.

Turbulence flow conditioning is by means of screens and

honeycombs. See Figure 2. Each stream first passed through a 40% blockage plate with 1.27 cm holes into a 25 x 20 cm rectangular duct. At 127 cm upstream of the splitter plate, honeycomb grids with 0.63 cm squares were inserted to break up the large scales of turbulence. This was followed by two 30 mesh screens with 0.33 mm diameter wires at 107 and 97 cm upstream of the splitter plate. The flow area then under goes a 5 to 1 contraction in a two dimensional nozzle which reduces the normalized turbulence intensity further. The shape of the nozzle was defined by the two arc method as done in Hermanson's experiment[2].

The two streams meet inside the test section at the splitter plate with a 6 degree convergence angle. The plate is made of a Haynes alloy to resist the high temperature, and the tip was cut to 0.2 mm thick to prevent edge ripple.

The test section is a pressure housing rated for 4 atmospheres, absolute. It is 10 cm high by 20 cm wide at the splitter plate tip and extends about 63 cm downstream. The upper and lower walls are moveable and are hinged about the upstream end, allowing the cross-section of the duct to be changed so that the axial pressure gradient can be adjusted to zero; these walls are convectively cooled with the slave air.

The two side walls each contain two quartz windows with individual viewing areas of 8.5 x 21.5 cm. They are air-cooled, each with a 0.48 cm wide film slot beginning at the upstream edge of the windows and covering the complete height of the windows. These windows allow optical access for LDV and imaging cameras. The first set of windows includes about 4.5 cm of the splitter plate so that the upstream boundaries can be observed and measured. Using the splitter plate tip as the origin, the two viewing areas cover from x= -4.5 to 17.0 cm and then x= 26.0 to 47.5 cm.

Metal plates with servomotor-placed thermocouples were substituted for the windows to determine the temperature distribution across the vertical midplane of the shear layers.

The test section is followed by a smooth transition section from a rectangular cross section at the test section outlet to a 45 cm diameter round area where back pressure tubes can be inserted for operating at elevated pressures. In the exhaust, water sprays cool the gases that are expelled over the test cell roof.

2.2 DIAGNOSTICS

2.2.1 VELOCITY MEASUREMENT

A two-component, forward-scatter heterodyne laser Doppler velocimeter system was used to measure the streamwise and cross-stream flow components in the planar reacting shear layer duct. A 5 W Coherent Innova 90 argon ion laser operating in the multiline mode provided the illumination. The 488.0 nm blue line was used to measure the (horizontal) streamwise velocity component, u, and the 514.5 nm green line was used to measure the (vertical) cross-stream component, v. Laser beam output diameter was 1.5 mm.

The transmission optics were arranged on a 61 x 183 cm breadboard, essentially as a TSI Model 9100-7 four beam system. The multiline emission was separated using a prism color separator before the green (514.5 nm) and the blue (488.0 nm) beams were sent through separate beam splitter crystals. Beam separation distance was 50 mm.

An achromatic lens (d=60 mm) with 602 mm focal length focused the four beams into the test section centerline via the large 10 x 20 cm windows. For the the green beams, the waist was 262 microns, 6.3 mm long, and fringe width was 6.18 microns. For the blue, the waist was 250 microns, 6.0 mm long, and fringe width was 5.86 microns. For the cross-stream component, V, a 40 MHz shift was added through a Bragg cell since flow reversal is possible in this direction; no frequency shift was used for the streamwise component, U.

The receiving optics were arranged on a 61 x 61 cm breadboard on the other side of the test section. The elements for the two color components were separated to optimize the amount of light collected. Each train consists of a receiving lens, an integral assembly containing a 100 mm focusing lens, a narrow band color filter, and a two axis traverse adjustment. A photomultiplier tube (PMT) with a 175 micron diameter pinhole is attached to each train to collect the light. Each train is placed at an angle of ten degrees off axis in order to avoid having the incident laser beam shining directly into the PMTs. An $f9$ 350 mm focal length lens was used to collect the blue light and an $f11$ 450 mm focal length lens was used to collect the green light.

The signal from the blue PMT was sent directly to a TSI model 1990 burst counter processor; the PMT signal of the frequency shifted green light was first sent back into a downmixer (removing 30 MHz) and then sent to the processor. The transmission lines from the PMTs in the test cell to the processors inside the control room are a pair of 30 m long RG58 coaxial cables.

The TSI counters are normally set to constant settings for the duration of the experiment once the computer controlled mapping starts. The filter amplifier gains are usually set between 1x and 2x. The blue color cutoff frequencies are 20 MHz and 100 MHz. The green cutoff frequencies are 2 MHz and 20 MHz. Outputs of the signals are via the counters' analog frequency outputs with 12-bit resolution. They are linearly proportional to the detected Doppler frequencies and hence the velocity components. The analog signals are sent to a sample and hold board and then a 12-bit A/D board on the Concurrent 5600 data acquisition computer. The sampling rate is fixed at 20 kHz per channel.

Flow speeds at various locations from the splitter plate tip to 330 mm downstream were measured. The measurement probe volume was moved relative to the test section by driving the whole optics table using stepper motors controlled by a CompuMotor 4000 controller. This in turn was controlled remotely by the Concurrent 5600 which controls the positioning of the measurement location as well as the high-speed data acquisition. The data acquisition and control software were custom written by the authors. Typical cycling time was about 7 seconds per location, of which only 4 seconds were data acquisition (2 seconds for the non-reacting case). The rest was occupied by table traverse and stabilization. The total mapping cycle covering the two sets of windows took about 30 minutes. This is usually the maximum length of the mapping time since the seeders rarely worked well longer than 30 minutes.

Various types of seeds were used to scatter the incident laser beams, but a mixture of 20% fumigated silica and 80% alumina of nominally 1 micron diameter was eventually adopted as standard. (Attempts at using titanium dioxide formed from titanium tetrachloride and steam reaction were unsuccessful and the technique was abandoned.) The powder mixture is first heated in an oven to 470 K for an hour to dry the powder, and then it is poured into the two seeders, one each for the fuel duct and the air duct.

The seeder design used features from fluidized beds and cyclone separators. The cylindrical seeders were made with 15 cm diameter and 60 cm long steel pipes, capped at the top and bottom with end caps. The latter were attached to the pipe with standard flexible seals for quick release. Dried nitrogen is introduced in the center of the bottom cap and enters the bottom of the mixing chamber through a wire mesh and sintered metal plate such that the gas moving upward through the 5 cm thick seed bed agitated the seeds. Two small nozzles about 5 cm from the bottom of the bed inject air tangentially into the fluidized bed chamber so that larger particles are spun to the side and attach themselves to the wall as the bulk flow rises. The particle-laden flow is siphoned off the center of the top cap and ducted (via a copper tube) to a 1.2 cm diameter probe inserted into the main ducts upstream of the honeycombs. During operation, the carrier nitrogen pressure normally was set to 420 kPa.

2.2.2 TEMPERATURE MEASUREMENTS

The temperature profiles across the shear layer (in the vertical direction, y) at x=300 mm were measured with 0.625 mm diameter type R wire thermocouple probes. Due to the large thermal inertia of the junction, the traverse had to be done slowly. The typical traverse speed was about 0.2-0.4 mm/s to reduce error introduced by thermal inertia.

2.2.3 OTHER INSTRUMENTATIONS

A standard Schlieren system capable of observing a whole window was used in conjunction with a 10,000 frame per second high-speed film camera to capture instantaneous density gradient distribution. An intensified, gated, 2-D array camera is used to measure OH fluorescence as well as planar Mie scattering from a pulsed laser. High frequency microphones are used to measure pressure boundary conditions. Details on these are beyond the scope of this report, and readers are referred to Reference 10.

2.3 OPERATING CONDITIONS

The nominal control settings and measured flow conditions are given in Table 1. The upper fuel stream with nitrogen diluted hydrogen was replaced with air for the non-reacting case. The velocity ratio was fixed nominally at 0.34 for all experiments.

3

2.4 ERROR ANALYSIS

Uncertainty in the fringe width and hence the scaling value to convert the signal from frequency into absolute flow speed is 0.4%. However, since this uncertainty affects the whole of the data set equally, it does not alter the normalized characteristics of the data. Quantities such as normalized turbulence intensity, spectral densities, and scales are not affected.

Signal leakage of one component into the other because the two components are not orthogonal is not assessable, and it is assumed it to be limited by the accuracy of TSI-manufactured components. For example, for our 400 m/s mean flow in the streamwise direction, only a 2.3 degree misalignment is necessary to cause a 16 m/s mean flow to appear in the cross-stream direction component.

It is well known that the signal gain setting on the TSI burst counter processors can affect the measured absolute turbulence intensity. As the gain is increased, signals and noise from smaller particles are accepted by the processor as valid results, thus manifesting itself as higher data rates. This was not assessed as it is a function of the nature of the seed size distribution, nominally rated at 1 micron diameter. However, this uncertainty is more sensitive in the lower level turbulence of the inlet freestream flows. Assuming the inlet turbulence is isotropic, then about 25% error in the measured inlet turbulence intensities can be expected.

Signal discretization introduced about a 0.01% error with the 12-bit digitizer. In physical values, the u and v component have uncertainties of 5.5 and 1.4 cm/s respectively.

The effect of beam steering due to flowfield temperature changes on the signal was not noticeable. This may be attributed to the normal incidence angle formed between the side windows and the optical axis, along with the shallow convergence angles of the incident laser beams which minimized the misalignment of the focal points of the transmission and the receiving components. However, the radiative heating effect on the table has more than once caused the optic system to be misaligned such that one or both of the signals disappeared completely. This was corrected by installing radiation shields on the table.

No vibration of the optics components was noticed. The optics table was examined with accelerometers and was found to have no detectable displacement. The vibration of the rig itself was barely noticeable by physical touch, and the amplitude was judged to be less than 0.5 mm in the 30 Hz range.

The greatest source of random noise comes from ground loop and electromagnetic interference from coupled electronic instruments. During operation, noise levels of about 20 mV from the analog output of the counter processor to the digitizer board on the computer can be detected. This corresponds to roughly 1 m/s random noise on u and 1/4 m/s on v.

Velocity measurement error due to particle mistrack is at most 3% of the local RMS turbulence level.

Velocity bias due to unequal particle seeding density in the two streams is compensated for by using time averages instead of particle averages.

The standard error for velocity measurement at any location is at most 1/90 of the corresponding measured turbulence level, or 0.5 m/s in U and 0.2 in V . This is the result of collecting at least 8000 samples; some locations had more than 60,000 samples in 4 seconds, and there the standard errors reduce by the square root of the corresponding number of samples.

Flow rate fluctuations in the data acquisition period were maintained to within ±0.6% of the mean, peak to peak.

The positioning uncertainty due to thermal expansion of the rig is about 0.5 mm vertically. As much as 5 mm of displacement of the test section in other occasions has been noticed. In the burning case, there was a spatial uncertainty regarding the exact location of the splitter plate tip (the origin) after the LDV data scan. This uncertainty is corrected using the U profile at the x=0 station as the guide. Apparently, the extra heating due to hydrogen combustion caused the rig to bow and displace slightly, for this was not observed similarly in the non-reacting hot air case. This spatial uncertainty is not present in the thermocouple measurements since the thermocouple translation mechanisms are fixed to the test section directly.

2.5 COORDINATE CONVENTION

A three axis Cartesian coordinate system was defined with the origin at the tip of the splitter plate, at the centerline of the duct. The x coordinates are positive towards downstream. The y coordinate is positive upward. The z component, across the width of the shear layer, is not used.

3. RESULTS AND DISCUSSION

3.1 OBSERVATIONS

A slightly yellowish glow was noticed in the mixing zone where combustion took place. The consensus opinion of the research personnel was that the hydrogen fuel from the bulk trailer was contaminated with sodium which is typical of this source.

Secondly, the temperatures of the two streams were not high enough to ensure spontaneous and sustained ignition inside the test section. To overcome this, 0.0022 Kg/s of the total hydrogen flow was diverted into the heated air duct to fuel a hydrogen torch. This created a slightly uneven temperature distribution inside the air nozzle. Figure 3 shows the temperature profiles taken at the x=300 mm station, showing that a temperature rise of about 180 K was present for a significant distance across the layer. This, unfortunately, increased the incident turbulence in the hot air stream to about 6 -7%.

Data rates fluctuated throughout the 30 minute data acquisition cycle as well as with location of measurement.

This is typical of the non-homogeneous nature of the seeding process. The counter processors indicated data rates as high as 130 kHz per channel, but the excess data were not used since the computer was sampling only at the fixed 20 kHz. Where the data rate was lower, the computer recorded the zeroth order hold nature of the processors' analog outputs as a series of steps. The sampling rates and sampling times are in Table 1.

The acoustical signature with and without reaction was different. In the presence of the non-reacting shear layer, a high-frequency hiss was heard in the control room. Microphone measurements have recorded wide-band dynamic pressures inside the test section as high as 550 Pa[10]. When ignition in the shear layer was stabilized, the dynamic pressure roughly doubled and the tone was deeper, suggesting a larger portion of the turbulence energy is distributed in the larger scale eddys.

3.2 STREAMWISE VELOCITY COMPONENT, U

The mean streamwise velocity component, U, for the two shear layers at the same initial flow speeds are shown in Figure 4. The free stream speed remained stable for the non-reacting case, but decreased slightly for the reacting case due to the slightly divergent channel, to about 10% less at x=150 mm station. Also, in the reacting flow case, the free stream speed at the cold fuel side was not measurable at x=300 and 330 mm stations due to the displacement of the layer towards the low speed side.

Velocity profiles for both cases are self-similar by normalizing the cross-stream coordinates using the local layer vorticity thickness based on the shear layer slip velocity. They collapsed into two curves (see Figure 5), thus suggesting that the layer is dominated by the shearing of the two streams. The collapsed curves were best represented by the error function (ERF), also drawn on the same plot as a reference. The curve fit is not perfect, however, since the high speed side tends to have slightly steeper corner as was observed by Hermanson[2]. Nevertheless, this feature is well within the data scatter.

The exception to this was the small deviation detected at the x=6 mm station[†], this being the result of momentum deficiency introduced by the boundary layers from the splitter plate. Since this station is within the development length of 12 mm based on the Reynolds number criterion as specified by Goebel and Dutton[8], this deficiency is expected.

3.3 TURBULENCE AND DIFFUSION

The distribution of absolute turbulence intensities for the streamwise direction, u', and that for the cross-stream direction, v', are shown in Figure 6. The measured inlet intensities in the non-reacting case, normalized by the local U, are about 2.5% and 3%, about two times higher than

---

† The small convergence angle of the transmitted laser beams required a clearance of about 5 mm. Measurements at x= 0 mm detoured around the splitter plate tip with a radius of 6 mm. Thus the closest location mapped on the centerline was at 6 mm downstream of the splitter plate tip.

originally designed. The corresponding values are 4% and 5.6% for the reacting case. The much higher turbulence in the high-speed air duct is produced by the addition of the hydrogen torch. Note that the free stream turbulence in both inlets for the non-reacting case is approximately the same size, suggesting that isotropic turbulence is a reasonable assumption as an inlet boundary condition. In the presence of the hydrogen torch, however, it is not.

Under the non-reacting condition, the u' profiles exhibit bell-shaped curves about the shear layer whereas those in the case with reaction are much more difficult to characterize due to the distortion of additional turbulence from the torch. However, the peak streamwise turbulence at each station is about the same for the two cases, although the peaks in the reacting case tend to be broader and moved toward the slower speed side. This corresponds to the shift of the layer as seen Figure 4.

The cross-stream turbulence, v', did not vary as much as u' across the layer. Whereas there seems to be a slight increase in the center of the shear layer in the more upstream stations, those at 300 mm and 330 mm are nearly flat in the non-reacting case. This suggests the lack of an organized transport process to transfer turbulent energy from u' to v'. Of course, the turbulence is highly non-isotropic inside the shear layer, with u' to v' at roughly a ratio of three in the middle of the layer.

The Reynolds stresses normalized with respect to the the turbulence components u' and v' are generally small in the incident flows (Figure 7), which is expected in isotropic freestream flows. Without reaction, the values remained small and disorganized throughout the length of the shear layer, suggesting either the lack of large scale coherent structures, or that the larger scales are overshadowed by the more chaotic smaller scale motions.

With the presence of combustion, however, slightly larger values were detected at all downstream locations of x > 25 mm with values ranging from -0.15 to 0.2.. A trend of larger positive values in the middle of the shear layer appeared beginning at x=100 and became more organized as the shear layer moved downstream. This positive value corresponds to the faster fluid moving upward and the slower fluid moving downward, suggesting the presence of a larger scale momentum exchange, perhaps even a vortex type of entrainment process. Schlieren photographs taken[10] (reprinted here as Figure 8) show the presence of large scale structures that are related to the layer undulating in the streamwise direction; this feature is apparently absent without reaction. In the same manner, the somewhat small but organized negative values at downstream stations of x>25 mm may represent the diffusion of high-speed fluid moving into slower fluids near the diverging bottom wall.

3.4 LAYER GROWTH RATE

The mixing layer boundaries based upon the vorticity thickness of the layer are presented in Figure 9 for both cases. The mixing layer angles with and without reaction are about 8.1° and 6.1° respectively, averaged from x=50 mm to x=300 mm with the latter comparing favorably with the prediction based upon the formulation of Dimotakis[11] of

5.5°. The layer growth rate with heat release, however, was much larger than expected. This seems to be contrary to the observation of Wallace[6] and Hermanson[2], where the maximum velocity gradient steepened with reaction instead of being flattened here.

Also different is the shift of the shear layer into the slower fuel stream when reaction is present; not only did the centerline shift, both edges shifted as well. See Figure 9. No simple explanation is adequate. For example, one theory on this is that the torch somehow provided an initial upward flow along the centerline of the test section, and this upward motion continued throughout the length of the shear layer, as can be seen in Figure 10. This is certainly a plausible explanation in view that the shear layer transit time to traverse the 300 mm at the median flow speed of 270 m/s is about 1.1 ms. For an average upward motion of 16 m/s, the middle of the layer is displaced 18 mm during this same period. However, a review of the Schlieren photographs shows that the mean layer position shifted towards the test section horizontal centerline when the main hydrogen is turned off, even while the torch is left on. Turning the torch off (equivalent to the non-reacting case) does not make a noticeable further shift. Thus, the presence of the torch alone is insufficient to explain the shift of the reacting shear layer towards the slower fuel side.

3.5 PROBABILITY DENSITY FUNCTION (PDF)

The PDFs of the two velocity components in regions outside the shear layers show normal Gaussian distribution about the mean flow speed. Inside, however, the distribution becomes heavily skewed due to the entrainment of fluid from the other stream. Figure 11A shows one such distribution across the width of the mixing layer at x=100 mm. This same behavior is retained in the presence of reaction and is shown in Figure 11B. As the flow moved downstream, more of the cross-stream locations developed into the non-Gaussian distribution that is common inside a shear layer which corresponds to the growth of the layer width.

The PDF of the cross-stream component, v, remains approximately Gaussian throughout the flow, even inside the shear layer, for both the reacting and the non-reacting cases.

Joint PDF of u and v show no distinctive axis of alignment throughout the freestream. Inside the shear layer, no definitive pattern emerged for the non-reacting air to air flow. With reaction, a slight alignment occurs inside the shear layer at downstream locations. This observation is consistent with the slightly positive Reynolds Stress measured at downstream stations and corroborates with the development of organized turbulent transport inside the shear layer for the reacting case.

3.6 THERMAL PROFILE AT x=300 mm

Thermal layer thickness for the hot air shear layer was 38.4 mm at the x=300 mm location. It is based on the vorticity concept using the maximum thermal gradient found in the middle of the layer. With reaction, it is about 53 mm[†]. For the non-reacting flow, median temperature is reached at

y=6 mm, and the maximum temperature increase with reaction is registered at y=11 mm. Both of these locations are significantly far away from the midpoint of the corresponding momentum layers, which are at y=-2 mm and y=18 mm respectively.

4. GENERAL DISCUSSION

While the non-reacting shear layer grew at about the same rate as predicted[11], the reacting shear layer grew at a much faster rate. One possible explanation to this difference is that the divergence of the upper and lower walls to the test section slowed down the flow, set up a adverse pressure gradient and caused the mixing layer to grow at a faster rate. However, our transducers monitoring the test section pressures did not indicate this.

The growth rates for both of these cases, however, still fall within the established limits. The convective Mach numbers, M_c, in our reacting and non-reacting cases are 0.26 and 0.29. These correspond to δ_c/δ_i[‡] of 0.90 in Figure 4 of Messersmith et al.[12], meaning that our mixing layer is practically incompressible even though the two incident streams themselves were moving in the compressible regime. From the incompressible plot of δ_i vs. $\Delta U/U_m$ (Figure 5 in Ref. 12), the growth rates of our reacting and non-reacting layers of 0.14 and 0.11 are found to fall near the upper edge of the data scatter, which ranges from 0.09 to 0.14.

In both cases, the velocity profiles collapse onto the ERF curve. Without reaction, the thermal profile also fitted ERF as well. Since both the thermal and velocity profiles can be represented by ERF, turbulent entrainment is assumed to be the main mechanism by which elements from the two streams are brought together to react. Thus, the ratio of the momentum and the thermal layers can be used to form a turbulent Prandtl number for each case. These are 0.77 and 0.83 for the flows with and without reaction, a significant departure from Batt's 0.5.

The thermocouple data for the reacting case shows significant heat release due to combustion in the mixing layer. The long dashed line in Figure 3 shows a peak temperature rise of about 810 K. Using the turbulent Schmidt number of 0.77 to approximate the species distribution inside the layer, an approximate adiabatic temperature profile is shown here as the short dashed curve in Figure 3. It is about 250 K higher than the measured temperature peak with reaction, suggesting that perhaps about 70% of the reactants have been consumed. This proportion will increase with radiation loss correction for the thermocouples added, since the temperature difference will be less.

Heat release apparently increases the level of larger scale turbulence. The extent of increase to scales on the order of the layer thickness is debatable among the authors, but Schlieren photographs of the reacting shear layer in Figure

---

† This is obtained by extending the tangents to the maximum slopes of the two sides of the temperature difference curve in Figure 3 - result of taking the difference of the burning case and the torch case - to where these tangents intersect the base.

‡ This is the ratio of layer growth rate of a compressible shear layer to that of an incompressible shear layer.

8 clearly show the presence of large scale corrugation of the shear layer, in some respect akin to a traveling wave. This type of behavior is coherent and correlatable, and can be used to explain the origin of the small but organized Reynolds stress in Figure 7. Assuming that only this larger scale motion is coherent, then the ~ 25% cross-correlation coefficients in the u' and v' components from the last three downstream stations in Figure 7 suggest that about 25% of the turbulence energy measured in the reacting flow can be associated with these large scale structures, compared to only about 10% in the non-reacting flow.

The changes in the finer flow scales inside the layers are indeterminate from the present set of LDV data alone. The maximum 20 kHz data rate is only able to resolve length scales over 4 cm at 400 m/s mean flow speed. This size is larger than the mixing layer thickness for the first 200 mm of the layer, and so is not meaningful in providing information regarding the smaller scales inside the layer itself. That information must come from flow visualization techniques.

5. CONCLUSIONS

Statistical values of measured velocity, turbulence, and temperature profiles were obtained at Mach number of 0.71 with and without combustion. However, the low convective Mach numbers of 0.29 and 0.26 mean that these cases can be treated as incompressible. Even with combustion the error function fit the reduced velocity profile fairly well, suggesting that the shear layer is dominated by the shear of the two freestreams. Combustion in the shear layer accelerates the shear layer growth rate and shifts the layer towards the lower speed side. It apparently also increased the larger scale turbulence, in this case the undulation of the shear layer itself, and increased slightly the organization of turbulent energy transport from the streamwise direction to the cross-stream.

TABLE 1: FLOW CONDITIONS

Nominal Values	Non-Reacting	Reacting
Air stream flow	1.87 Kg/s @824K	1.94 Kg/s @817 K
Fuel stream air	1.62 Kg/s @303K	- none -
Fuel stream N_2	- none -	1.00 Kg/s @348 K
Fuel stream H_2	- none -	0.032 Kg/s @348 K
Pressure	1.000×10^5 Pa	1.063×10^5 Pa
Upper flapper	parallel	1.3° divergent
Lower flapper	parallel	1.3° divergent

Measured and Calculated Values		
Air speed, U_1	394 m/s	390 m/s
Fuel speed, U_2	134 m/s	137 m/s
Air side density, ρ_1	0.46 Kg/m³	0.50 Kg/m³
Fuel side density, ρ_2	1.18 Kg/m³	0.74 Kg/m³
Air stream M_1	0.72	0.71
Fuel stream M_2	0.39	0.30
U_2/U_1	0.34	0.34
ρ_2/ρ_1	2.57	1.48
$(\rho_2 U_2)/(\rho_1 U_1)$	0.87	0.51
$(\rho_2 U_2^2)/(\rho_1 U_1^2)$	0.30	0.18

† Based on the mixture of an unit volume from each inlet stream.

Conv. speed, U_c	298	297
Conv. Mach, M_c	0.29	0.26
Equiv. ratio†, Φ	0	1.60
Layer angles:		
Measured	6.1°	8.1°
Projected[2]	5.5°	4.9°‡
$\Delta U/U_m$	0.98	0.98
$\Delta T_{max}/T_{mean}$	0	1.46
Data rate	3 kHz-18 kHz	2 kHz-16 kHz
Sampling time	2 seconds	4 seconds

REFERENCES

1. Strahle, W.C. and S.G. Lekoudis,"Evaluation of Data on Simple Turbulent Reacting Flows", AFOSR-TR-85-0880, Sept. 1985. (Avail. NTIS, AD-A170071).

2. Hermanson, J.C., "Heat Release Effects in a Turbulent, Reacting Shear Layer", Ph.D. Thesis, California Institute of Technology, Pasadena, California, 1985.

3. Claus, R.W., "Modeling Turbulent, Reacting Flow", Combustion Fundamentals, NASA CP-2433, NASA-Chinese Aeronautical Establishment (CAE) Symposium, Cleveland, Ohio, September, 1986.

4. Farshchi, M.,"Prediction of Heat Release Effects on a Mixing Layer", AIAA-86-0058, AIAA 24th Aerospace Sciences Meeting, Reno, NV, 1986.

5. Batt, R.G.,"Turbulent Mixing of Passive and Chemically Reacting Species in a Low-Speed Shear Layer", J. Fluid Mech., v.82, 1977, pp. 53-95.

6. Wallace, A.K., "Experimental Investigation on the Effects of Chemical Heat Release in the Reacting Turbulent Plane Shear Layer", Ph.D. Thesis, The University of Adelaide, 1981. Available as AFOSR-TR-84-0650.

7. Clemens, N.T., P.H. Paul, M.G. Mungal, and R.K. Hanson, "Scaler Mixing in the Supersonic Shear Layer", AIAA-91-1720, AIAA 22nd Fluid Dynamics, Plasma Dynamics & Lasers Conference, Honolulu, Hawaii, 1991.

8. Goebel, S.G., and J.C. Dutton, H. Krier, and J.P. Renie,: "Mean and Turbulent Velocity Measurements of Supersonic Mixing Layers", Experiments in Fluids, v.8, 1990. pp.263-272.

9. Hall, J., P.E. Dimotakis, and H. Roseman, "Experiments in Non-Reacting Compressible Shear Layers," AIAA-91-0629, 29th Aerospace Sciences Meeting, Reno, NV, 1991.

10. Chang, C.T., C.J. Marek, C.C. Wey, C. Wey, "Experimental Reacting Hydrogen Shear Layer Data at High Subsonic Mach Number", NASA TP-3342, 1993. In print.

11. Dimotakis, P.E., "Entrainment into a Fully developed, Two-Dimensional Shear Layer", AIAA-84-0368, 22nd Aerospace Sciences Meeting, Reno, NV, 1984.

12. Messersmith, N.L., S.G. Goebel, W.H. Frantz, E.A. Krammer, J.P. Renie, J.C. Dutton, and H. Krier, "Experimental and Analytical Investigations of Supersonic Mixing Layers", AIAA-88-0702, AIAA 26th Aerospace Sciences Meeting, Reno, NV, 1988.

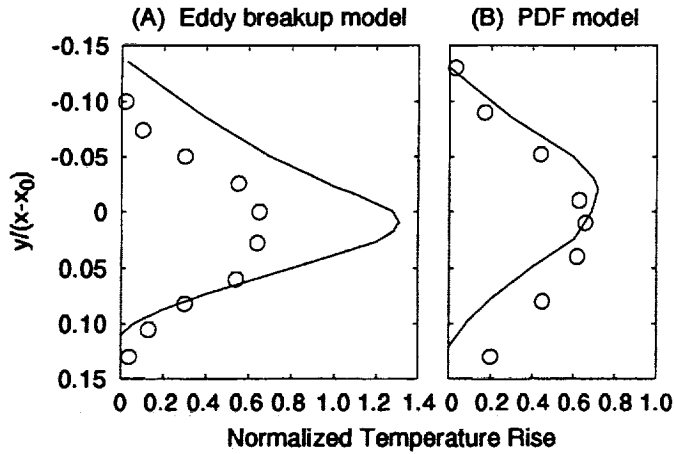‡ Estimate based on median temperature of the two inlet streams.

(A) Eddy breakup model   (B) PDF model

Figure 1 Comparison of Hermanson's data[2], open circles, with computations, lines.
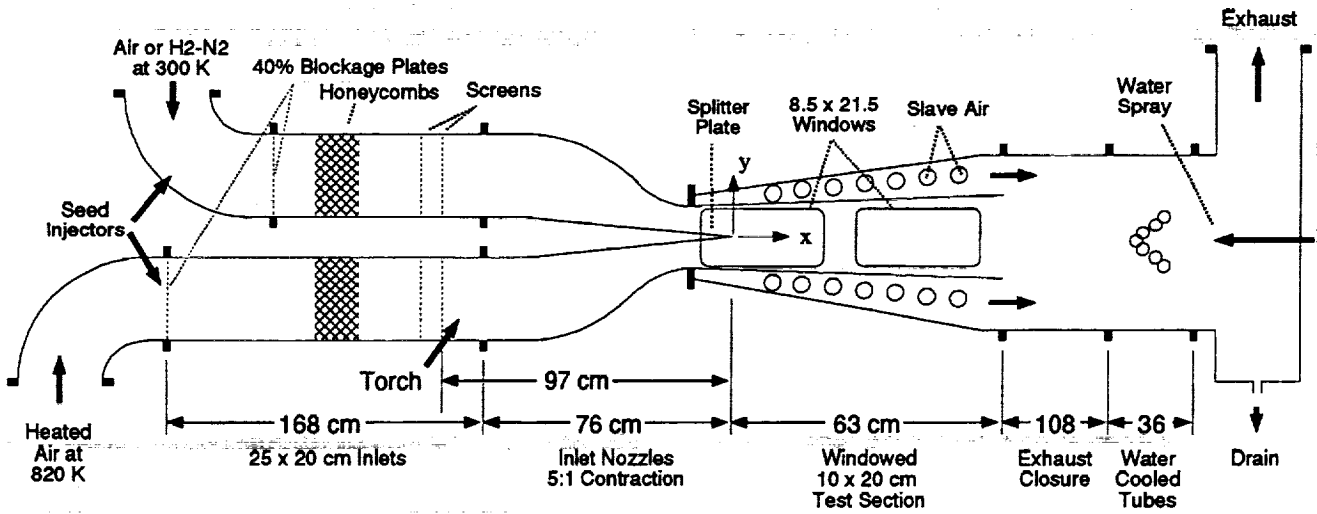(A) Eddy break-up model[3].
(B) Farshchi's PDF model[4].

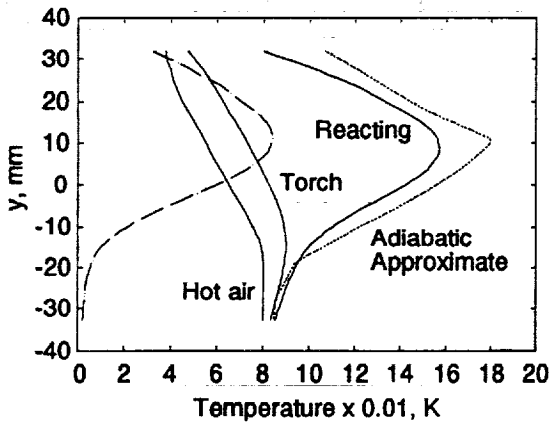Figure 2 Schematic diagram of Planar Reacting Shear Layer Facility

Figure 3 Temperature distribution in shear layer at x=300 mm station. Solid lines, measured temperatures, not compensated for radiation loss. Dotted line, approximate adiabatic temperatures. Long dashed line, temperature gain due to burning in shear layer.
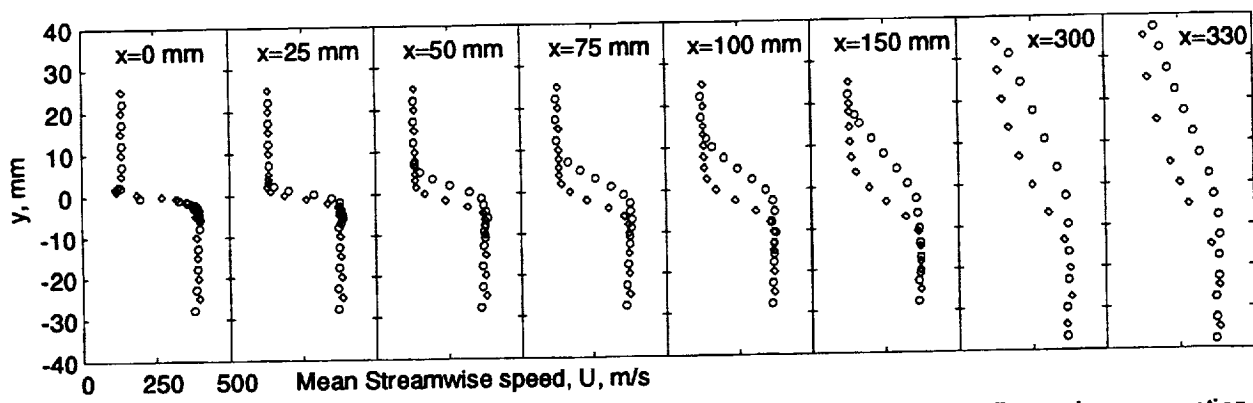
Figure 4 Mean streamwise velocity component at various stations. Circles, reacting; diamonds, non-reacting.

Symbol	x	$\delta_{\omega,n}$	$\delta_{\omega,b}$
×	0	1.81	1.15
△	25	3.39	2.94
◇	50	5.29	5.90
□	75	6.85	9.30
○	100	9.37	13.1
○	150	13.5	20.5
○	300	31.9	41.0
○	330	34.2	39.9
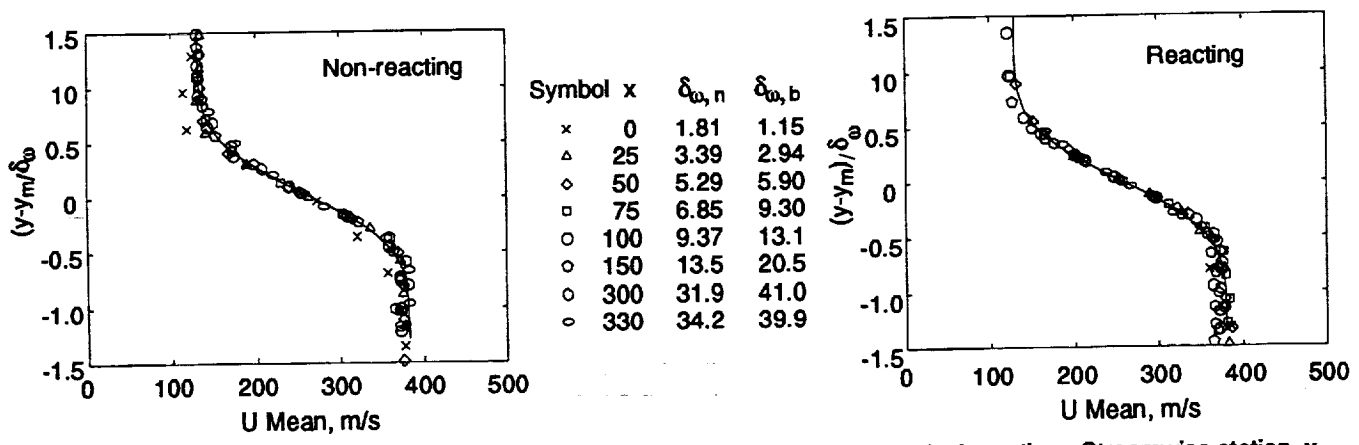
Figure 5 Collapsed mean streamwise velocity (U) profile with and without chemical reaction. Streamwise station, x, indicated by key at right side of plot, with local layer vorticity thickness indicated. Solid line, ERF.
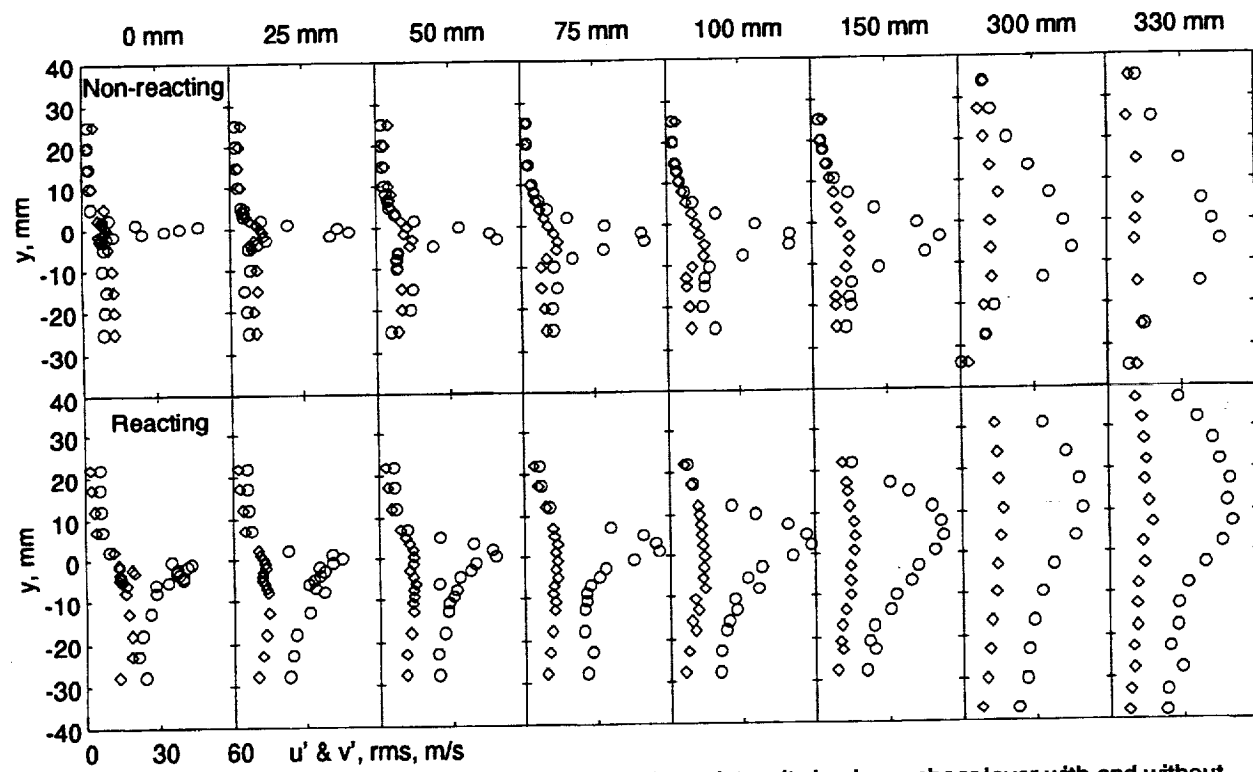
Figure 6 Streamwise and cross-stream absolute turbulence intensity in planar shear layer with and without chemical reaction. Circle, u'; diamonds, v'. Streamwise stations indicated at top.

9
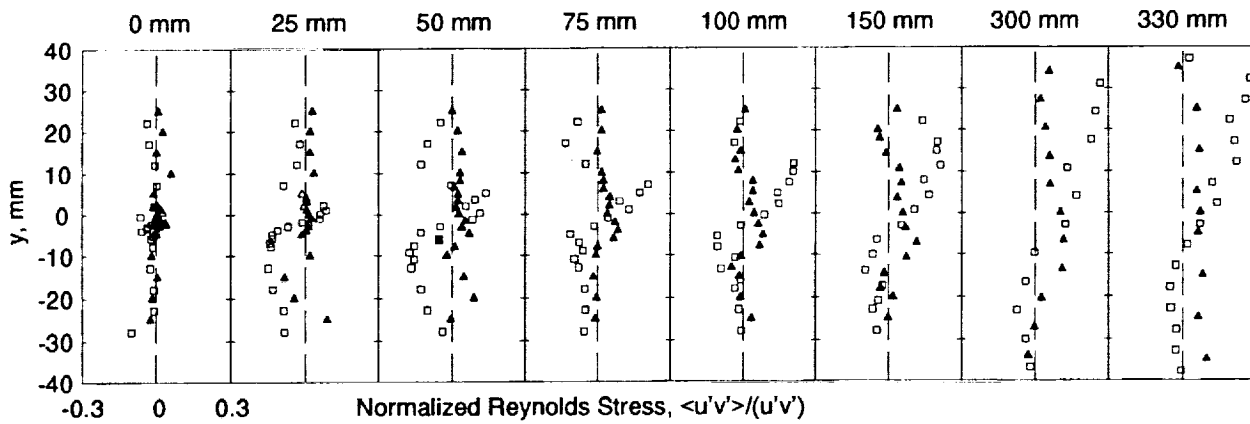
Figure 7 Reynolds stress normalized by local u' and v'. Squares, reacting; filled triangles, non-reacting. Streamwise locations marked on top of plots.
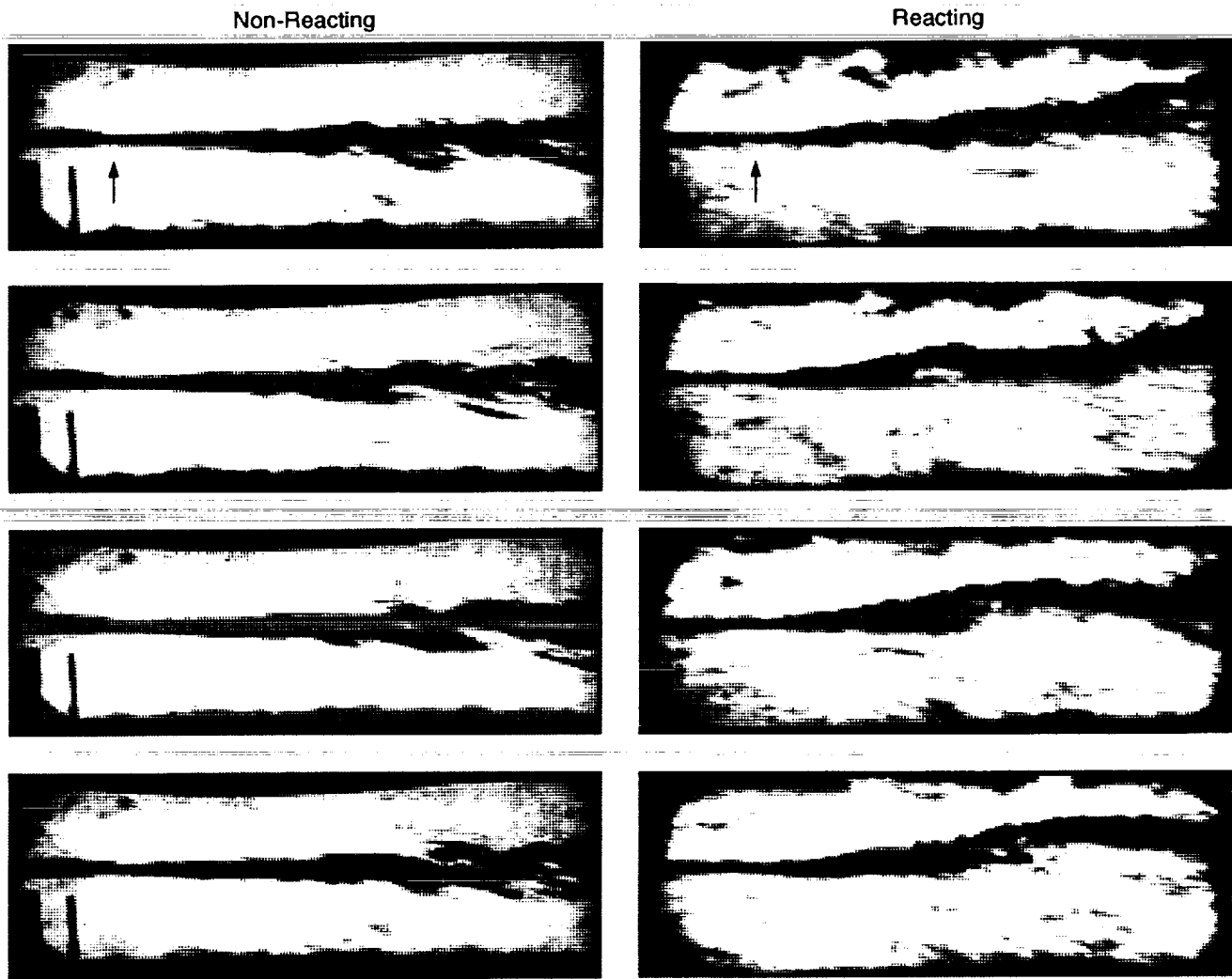
Figure 8 Schlieren photographs of reacting and non-reacting shear layers in the first set of windows. Arrows show the approximate location of the splitter plate tip. Successive frames are 100 μs apart. Left column, non-reacting, T_1=460 K, T_2=300 K. Right column, reacting, T_1=800 K, T_2=400 K. M_1=0.8, M_2=0.4.
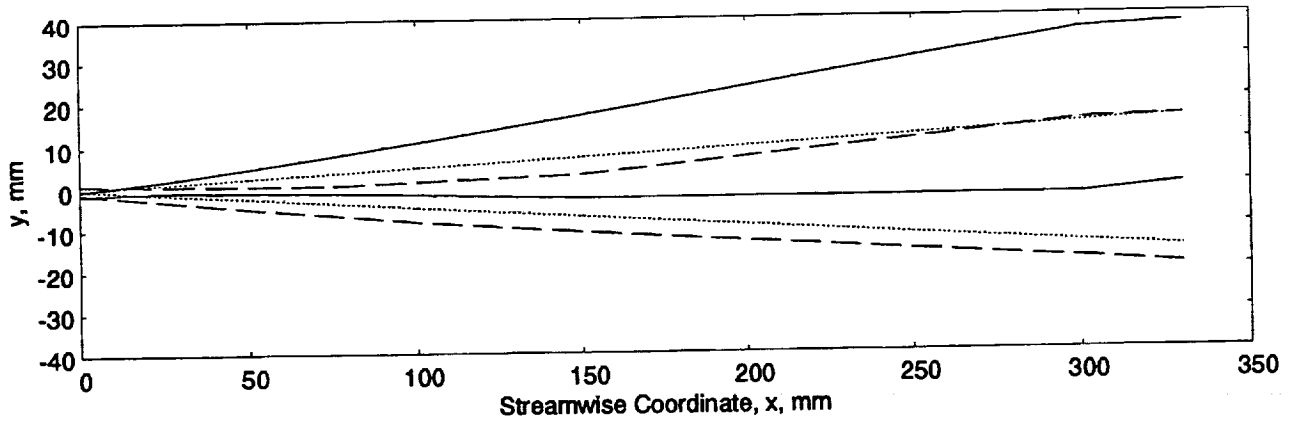
Figure 9 Shear layer vorticity thickness boundary. Solid line, reacting; long dash, non-reacting; dotted line, predicted non-reacting[11].
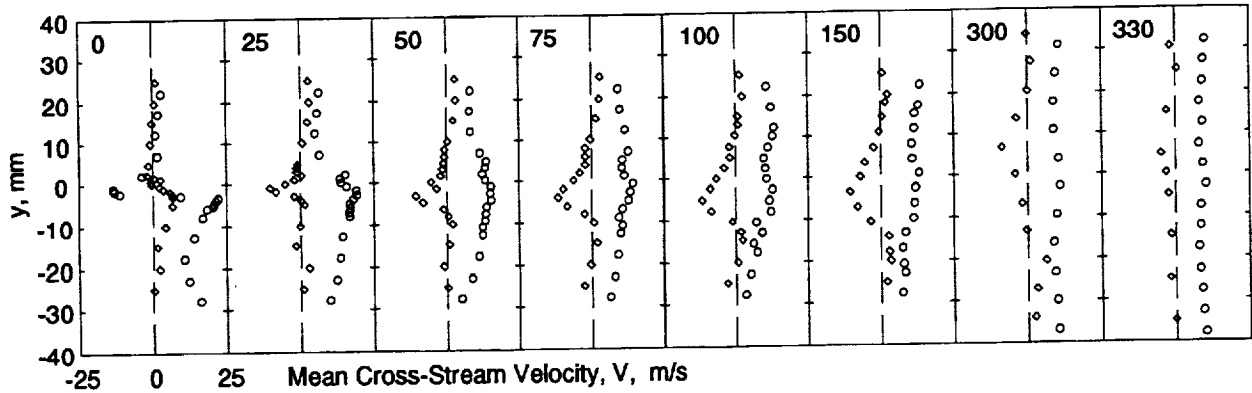
Figure 10 Mean cross-stream velocity in planar shear layer with (circle) and without (diamond) reaction at indicated stations.
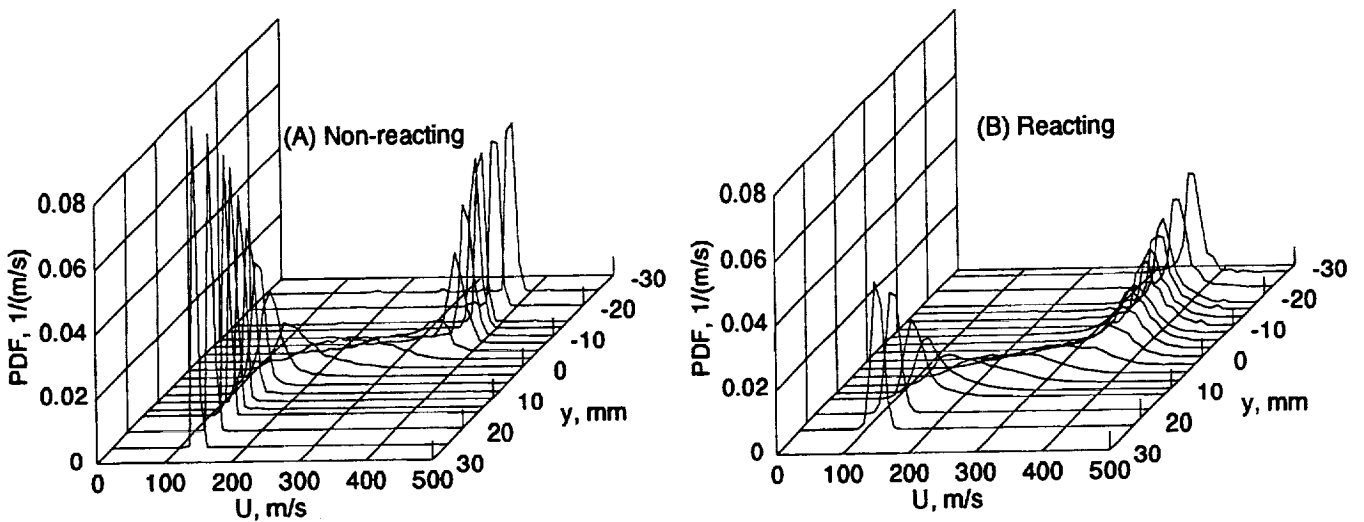

Figure 11 Streamwise velocity (U) Probability Density Distribution at x=100 mm station with and without chemical reaction.

REPORT DOCUMENTATION PAGE

Public reporting burden for this collection of information is estimated to average 1 hour per response, including the time for reviewing instructions, searching existing data sources, gathering and maintaining the data needed, and completing and reviewing the collection of information. Send comments regarding this burden estimate or any other aspect of this collection of information, including suggestions for reducing this burden, to Washington Headquarters Services, Directorate for Information Operations and Reports, 1215 Jefferson Davis Highway, Suite 1204, Arlington, VA 22202-4302, and to the Office of Management and Budget, Paperwork Reduction Project (0704-0188), Washington, DC 20503.

1. AGENCY USE ONLY (Leave blank)	2. REPORT DATE	3. REPORT TYPE AND DATES COVERED
	June 1993	Technical Memorandum

4. TITLE AND SUBTITLE

Comparison of Reacting and Non-Reacting Shear Layers at a High Subsonic Mach Number

5. FUNDING NUMBERS

WU–505–62–52

6. AUTHOR(S)

C.T. Chang, C.J. Marek, C. Wey, R.A. Jones, and M.J. Smith

7. PERFORMING ORGANIZATION NAME(S) AND ADDRESS(ES)

National Aeronautics and Space Administration
Lewis Research Center
Cleveland, Ohio 44135–3191

8. PERFORMING ORGANIZATION REPORT NUMBER

E–7905

9. SPONSORING/MONITORING AGENCY NAME(S) AND ADDRESS(ES)

National Aeronautics and Space Administration
Washington, D.C. 20546–0001

10. SPONSORING/MONITORING AGENCY REPORT NUMBER

NASA TM–106198
AIAA–93–2381

11. SUPPLEMENTARY NOTES

12a. DISTRIBUTION/AVAILABILITY STATEMENT

Unclassified - Unlimited
Subject Category 07

12b. DISTRIBUTION CODE

13. ABSTRACT (Maximum 200 words)

The flow field in a hydrogen-fueled planar reacting shear layer was measured with an LDV system and is compared with a similar air to air case without combustion. Measurements were made with a speed ratio of 0.34 with the high-speed stream at Mach 0.71. They show that the shear layer with reaction grows faster than one without, and both cases are within the range of data scatter presented by the established database. The coupling between the streamwise and the cross-stream turbulence components inside the shear layers is low, and reaction only increased it slightly. However, a more organized pattern of the Reynolds Stress is present in the reacting shear layer, possibly as a result of larger scale structure formation in the layer associated with heat release.

14. SUBJECT TERMS

Hydrogen; Combustion; Temperature; Turbulence; Velocity

15. NUMBER OF PAGES

13

16. PRICE CODE

A03

17. SECURITY CLASSIFICATION OF REPORT	18. SECURITY CLASSIFICATION OF THIS PAGE	19. SECURITY CLASSIFICATION OF ABSTRACT	20. LIMITATION OF ABSTRACT
Unclassified	Unclassified	Unclassified	